Research in Pharmaceutical Sciences, October 2025; 20(5): 651-666
Received: 08-12-2024
Peer Reviewed: 08-03-2025
Revised: 01-05-2025
Accepted: 03-06-2025
Published: 20-10-2025

School of Pharmacy & Pharmaceutical Sciences
Isfahan University of Medical Sciences

Original Article

Free-floating patient-derived organotypic tumor spheroids (PDOTS) from non-small cell lung cancer (NSCLC) tumors: a versatile tool for personalized testing of chemotherapeutic drugs

Lilian Ismail[1], Komal Zahid[1], Anna Polyanskaya[1], Aya Al Othman[1], Ningfei Shen[1], Xiaoli Qi[1], Rushan Sulimanov[1], Yuri Esakov[2], Vladimir Makarov[1], Gleb Filkov[1], Alexander Trofimenko[1], Alexandre Mezentsev[1], and Mikhail Durymanov[1,3,*]

[1]Medical Informatics Laboratory, Yaroslav-the-Wise Novgorod State University, Veliky Novgorod, Russia.
[2]Moscow State Budgetary Healthcare Institution "Moscow City Oncological Hospital No. 1", Moscow Healthcare Department, Moscow, Russia.
[3]Department of Radiochemistry, Faculty of Chemistry, M.V. Lomonosov Moscow State University, Moscow, Russia.

Abstract

Background and purpose: Patient-derived tumor 3D multicellular cultures are a novel non-small cell lung cancer (NSCLC) model for studying tumor biology and precision medicine, which recapitulates tumor morphology and gene expression profile. However, practical application is challenged by issues such as low establishment rates, long-term production difficulties, and the absence of immune microenvironment components. To address these issues, this study aimed to evaluate the efficacy of a novel method for generating free-floating patient-derived organotypic tumor spheroids (PDOTS) using a stimuli-responsive extracellular matrix (ECM)-mimicking gel.

Experimental approach: Free-floating PDOTS were established from 18 NSCLC tumors and characterized by their morphology, marker expression, and extracellular matrix composition. Cell composition in PDOTS and their parental tumors was analyzed by flow cytometry, while RT-PCR was used to assess the expression of genes encoding signaling molecules. Finally, drug response and the expression of drug resistance genes were evaluated in the NSCLC PDOTS.

Findings/Results: The PDOTS were successfully generated with a success rate exceeding 90%, forming spheroids within one week. These PDOTS preserved the parental tumor's morphology and included stromal and immune cells. Notably, 58% of the PDOTS maintained cytokine and growth factor expression profiles closely mimicked those of the original tumors. Furthermore, the PDOTS demonstrated varied responses to anticancer drugs, potentially influenced by differential expression of drug resistance-associated genes.

Conclusion and implications: The high establishment rate and rapid production timeline of free-floating PDOTS using a stimuli-responsive ECM-mimicking gel make this approach a promising tool for advancing cancer biology research and evaluating therapeutic strategies with greater accuracy.

Keywords: Cytokine; Drug resistance; Non-small cell lung cancer; Patient-derived organotypic tumor spheroids; Personalized medicine.

INTRODUCTION

Despite significant advances in treatment modalities in the last decade, lung cancer remains the first-ranked contributor to cancer-related deaths worldwide (1). Non-small cell lung cancer (NSCLC), with an approximately 15-20% 5-year survival rate, accounts for 80% of all lung cancer cases (2). Poor survival rate is partially attributed to the lack of an accurate prognostic method to evaluate treatment outcomes, which would help select a suitable experimentally-based treatment regimen for a certain patient.

*Corresponding author: M. Durymanov
Tel: +7-9773711758, Fax: +78162974526
Email: durymanov.mo@novsu.ru

Access this article online	
	Website: http://rps.mui.ac.ir
	DOI: 10.4103/RPS.RPS_233_24

Although genomics and transcriptomics have advanced precision medicine by linking genetic alterations and upregulated signaling pathways to targeted drugs (3), there are no reliable biomarkers for the prediction of tumor responses to chemotherapy (4), which remains a major treatment option for advanced NSCLC (5).

To address this concern, three-dimensional (3D) tumor-derived multicellular cultures, including patient-derived tumor organoids (PDTOs) and patient-derived organotypic tumor spheroids (PDOTS), have emerged as robust and reliable *in vitro* models for precision medicine (6,7). Increasing evidence confirms the phenotypic and genotypic correspondence between original tumor tissues and PDTOs/PDOTS across various cancers (8-10). Some clinical studies have demonstrated the high prognostic value of PDTOs/PDOTS for the evaluation of patient responses to targeted therapies and chemotherapeutic agents (11).

However, patient-derived spheroids and organoids have certain limitations, primarily due to technical constraints in their production techniques. The most common method of PDTO fabrication is based on embedding of tumor-isolated cells in MatrigelTM domes and their further incubation in the medium, encouraging growth of epithelial cells (7). This submersion technique typically produces spherical organoids that morphologically resemble tumor tissue but consist solely of epithelial cells and lack stromal and immune components that are crucial for certain applications, such as studying checkpoint blockade mechanisms (12). Another method is designed to produce PDTOs from micro pieces of tumor tissue, followed by their incorporation in collagen I gel and cultivation in an air-liquid culture system (13). Although this technique preserves immune and stromal components, it seems to provide non-uniform organoids that can be an obstacle to personalized drug testing. Compared to PDTOs, PDOTS generally retain stromal and immune components more effectively but exhibit limited morphological resemblance to the original tumor tissue. Most methods for producing PDOTS are based on the use of scaffolds (11,14), although a scaffold-free method has also been used (15). Nonetheless, the main challenges limiting the clinical integration of drug sensitivity testing using PDTOs or PDOTS include the low success rate of establishing viable 3D cultures and the prolonged time required for expanding organoids or spheroids from patient samples, which often takes weeks to months (16).

Here, we produced NSCLC PDOTS using a novel method, which has been tested earlier for the generation of highly fibrotic and more drug-resistant NSCLC spheroids (17). This approach exploits the embedding of tumor-isolated cells in stimuli-responsive extracellular matrix (ECM)-mimicking gel that allows for obtaining free-floating PDOTS in a short time. To date, no studies have evaluated the performance of this technique for NSCLC PDOTS generation. The primary goal of this study is to assess the efficiency of this method and characterize the resulting PDOTS.

MATERIALS AND METHODS

Human specimens

Small tissue fragments of 1 cm^3 volume were obtained from surgically resected lung specimens of both lung tumor tissues and non-neoplastic tissues. Histopathological examination definitively identified samples as either tumor or normal tissue. Expert pathologists confirmed the diagnosis for each case.

Generation of free-floating NSCLC PDOTS

Upon surgical resection, lung tumor tissues were immersed in DMEM/F12 (Gibco, USA) growth medium containing 1% PenStrep (PanEco, Moscow, Russia) and promptly transported to the laboratory on ice within 12 h. Next, the tumor tissues were sectioned into multiple pieces. One piece was embedded in HistoPrep tissue embedding media (Fisher Scientific, Ottawa, Canada), and kept frozen at -80 °C for further immunostaining. A second piece was preserved in RNeasy solution (Evrogen, Moscow, Russia) to enable subsequent total RNA isolation. A third piece was fixed in 10% buffered formalin (Thermo Fisher Scientific, USA) for H&E staining. Another piece was used for the preparation of tissue lysate for immunoblotting. The remaining tissue was finely minced using surgical scissors and suspended in 10 mL of

DMEM/F12 growth medium containing 1% PenStrep and 1 mg/mL collagenase I (Gibco, USA). Upon 1.5-h incubation at 37 °C with slow and gentle agitation, the digested tissue suspension was passed through a 70-µm cell strainer (Falcon, USA). The obtained cell suspension was centrifuged at 1,500 rpm for 5 min at 18-20 °C, followed by the pellet washing with Hanks' balanced salt solution (HBSS) and resuspension in 6 mL of fresh growth medium for spheroids (DMEM/F12 supplemented with 20 ng/mL of basic fibroblast growth factor (bFGF; 10014-HNAE, SinoBiological, China), 50 ng/mL human epidermal growth factor (EGF; ab55566, Abcam, UK), N_2 (PanEco, Moscow, Russia), NeuroMax (PanEco, Moscow, Russia), 10 mM Glutamax (Gibco, USA), 1 mM N-acetyl cysteine (Sigma, USA), 10 mM nicotinamide (Sigma), 10 µM Y27631 (ab120129, Abcam, UK), 15 µM HEPES (Sigma, USA) and 1% PenStrep). The cells were counted using a hemocytometer. A part of the collected cells was frozen for further flow cytometry analysis.

Free-floating NSCLC PDOTS were produced as described earlier (18). Briefly, 96-well plates were initially coated with 50 µL of a 1% w/v agarose solution in Milli-Q water. This coating was allowed to solidify at room temperature for approximately 20-30 min. Subsequently, a stimuli-responsive ECM-mimicking gel solution with resuspended tumor cells was prepared using SANATO 3D culture gel kit (#FTBM0051, Phystech Biomed, Russia) and 1% (v/v) SANATO reagent (#FTBM0050, Phystech Biomed, Russia) according to the manufacturer's protocol. Then, 25 µL gel domes containing 10,000-50,000 cells were dispensed into each well, and the gel was allowed to solidify at 37 °C for 20 min. After gelation, 100 µL of growth medium for spheroids was added to each well, and the plates were placed in an incubator, where they were cultured at 37 °C in a humidified atmosphere containing 5% CO_2. Growth medium was changed every other day throughout the entire experiment. The PDOTS were subjected to daily examination for 14 days, during which their size and morphology were observed using bright field microscopy with an AxioVert.A1 microscope (Zeiss, Oberkochen, Germany). PDOTS areas were determined in the brightfield images using ImageJ software (1.42v, US National Institutes of Health, USA). Measurements were performed on at least ten spheroids per time point.

Immunohistochemistry analysis

One-week-old free-floating NSCLC PDOTS were harvested, embedded into HistoPrep tissue embedding media (Fisher Scientific, Ottawa, Canada), and frozen at -20 °C. Subsequently, the frozen blocks with spheroids and original tumor tissues were cut into 10-µm-thick sections, fixed in the mixture of acetone and methanol (1:1) for 15 min, and air-dried at room temperature. Then, the slides were washed with Tris-buffered saline with Tween™ 20 (TBS-T) (1x) and kept in blocking solution for 1 h at room temperature. Then, samples were incubated with primary antibodies for 3 h at room temperature. To stain ECM components, rabbit monoclonal anti-fibronectin primary antibodies (ab2413, Abcam, UK), rabbit polyclonal anti-type I collagen antibodies (ab34710, Abcam, UK), and rabbit polyclonal anti-laminin antibodies (ab11575, Abcam, UK) were used. To stain other cell protein biomarkers, rabbit anti-PD-L1 (ab205921, Abcam, UK), anti-α-smooth muscle actin (α-SMA; ab124964, Abcam, UK), and anti-Ki-67 (ab15580, Abcam, UK) primary antibodies were used. After incubation with primary antibodies, the samples were washed with TBS-T and incubated with goat anti-rabbit IgG labeled with Alexa Fluor 488 (ab150077, Abcam, UK) for 1 h at room temperature. Nuclear DNA was stained with 4′,6-diamidino-2-phenylindole (DAPI) for 10 min before the samples were covered with a cover glass. The images of tumor tissue and spheroid sections were obtained using an inverted AxioVert A1 microscope (Zeiss, Oberkochen, Germany) equipped with a ×20/0.6 objective lens.

Western blotting

NSCLC PDOTS or tumor tissue lysates containing equal amounts of total protein (15 µg) were mixed with loading buffer, boiled for 5 min, separated by denaturing 12.5% sodium dodecyl sulfate (SDS)-polyacrylamide gel, and transferred to Amersham™ Hybond™ 0.45 µm

PVDF membrane (GE Healthcare, UK). The membrane was blocked for 1 h with a blocking buffer (Bio-Rad, Hercules, CA) under gentle agitation and incubated overnight with antibodies against E-cadherin (ES2220, ELK Biotechnology, China), thyroid transcription factor (TTF1; ab76013, Abcam) for adenocarcinomas, p63 (ab247245, Abcam, UK) for squamous cell carcinomas, or β-actin (ab8227, Abcam, UK) as a reference. Then, the membrane was washed twice with TBS-T and incubated with horseradish peroxidase (HRP)-conjugated secondary antibody (ab205718, Abcam, UK) at room temperature for 1 h, followed by several washings with TBS-T and deionized water. Protein bands were visualized by the ChemiDoc XRS+ imaging system (Bio-Rad, Hercules, CA) using chemiluminescence mode.

Flow cytometry

One-week-old NSCLC PDOTS were collected and treated with 1% collagenase I for 0.5-1 h at 37 °C. The cells, isolated from disintegrated spheroids, were washed with ice-cold Versene solution and used for sample preparation. Unfrozen cells, isolated earlier from the parental tumors, were also washed with ice-cold Versene solution and processed for sample preparation. The cell suspensions were stained with antibodies against well-established surface markers CD206 for M2-polarized tumor-associated macrophages, PD-L1 for an immunosuppressive fraction of cancer cells, and CD8 for cytotoxic T-cells using ab195192, ab205921, and ab17147 from Abcam, respectively. The samples, stained with anti-PD-L1 and anti-CD8 IgGs, were also treated with fluorescently labeled secondary antibodies (ab150113 and ab150115, Abcam, UK). Another sample was fixed in 4% paraformaldehyde with 0.1% Triton X-100, followed by staining with antibodies against α-SMA (ab124964, Abcam, UK) to determine myofibroblasts and secondary antibodies (ab150113, Abcam, UK). The staining was carried out at 1:100 and 1:200 antibody dilutions for the primary and secondary antibodies, respectively. To minimize non-specific IgG binding, the cell staining was performed in 1% bovine serum albumin (BSA) and 10% fetal bovine serum (FBS) solution. Unbound antibodies were removed by washing with phosphate-buffered saline (PBS). Recommended isotype controls were used as negative controls to exclude non-specific binding events. The cells were subjected to flow cytometry analysis using a CytoFLEX flow cytometer (Beckman Coulter, Brea, CA). Per sample, 10,000 events were gated.

RNA extraction and quantitative real-time polymerase chain reaction

Total RNA was isolated from PDOTS or tumors using the ExtractRNA kit (Evrogen, Moscow, Russia) in accordance with the manufacturer's protocol. The prepared samples were subjected to spectral analysis. If the absorption ratio A260/A280 was lower than 2.0, the samples were purified again using CleanRNA Standard (Evrogen, Moscow, Russia). cDNA was synthesized by random priming from 1 μg of total RNA using the MMLV RT kit (Evrogen, Moscow, Russia). These samples were subjected to quantitative polymerase chain reaction (qPCR) using CFX96 Real-Time PCR Detection System (Bio-Rad, Hercules, CA) with the primers listed in Table S1. For each reverse-transcribed sample, amplification of 18S rRNA served as an internal quantification standard. The results were analyzed using CFX Manager software supplied by the manufacturer. All samples were run in triplicate.

Cell viability assay

Viability of NSCLC PDOTS treated or non-treated with anticancer drugs was assessed using CellTiter-Glo® 3D Cell Viability Assay (Promega, Madison, WI) according to the manufacturer's protocol. Briefly, the spheroids were exposed to different concentrations of cisplatin, etoposide, pemetrexed, paclitaxel, or gemcitabine (all from Sigma, St. Louis, MO) for 96 h. Incubation of the PDOTS with drugs was carried out from day 7 to day 11. The final concentration of the drugs in wells ranged from 0 to 2 μM. After incubation with drugs, an equal volume of CellTiter-Glo® 3D reagent was added to the wells. Next, the plate was vigorously agitated for 5 min and incubated for an additional 25 min at room temperature in the dark. The luminescence was measured using a microplate reader CLARIOstar Plus (BMG LABTECH,

Ortenberg, Germany). All samples were tested in triplicate at each drug concentration.

Statistical analysis

The statistical data analysis was carried out using GraphPad Prism 5 (GraphPad Software Inc., San Diego, CA) software. Spheroid area and viability data are expressed as mean ± SD. All experiments were conducted in triplicate or more. To assess similarity between primary tumors and tumor-derived spheroids, correlation analyses were carried out. For each gene or protein of interest, correlations between RNA expression levels or biomarker-positive cell percentages in primary tumors and matched spheroids across patients were evaluated using Pearson's correlation coefficient (r). A *P*-value < 0.05 was considered statistically significant.

Supplementary materials

Additional supporting information is available at: https://github.com/Ukulele329/RPS_updated/blob/main/Supplementary%20Materials.docx.

RESULTS

Characterization of free-floating NSCLC spheroid morphology

The generation procedure of free-floating PDOTS resembles the conventional technique of PDTO production (Fig. 1A). Similarly, the isolated tumor cells were placed into an ECM-mimicking hydrogel, followed by incubation at standard conditions. At the same time, the gradual shrinkage of stimuli-responsive gel in the used technique encourages cell-to-cell connections and rapid formation of multicellular aggregations, which are becoming free-floating spheroids over time (Fig. 1B).

We obtained free-floating PDOTS from different types of NSCLC tumors, including adenocarcinoma, large-cell carcinoma, and squamous cell carcinoma (SCC) (Fig. S1A and Table S2). The usage of this technique allowed us to obtain free-floating spheroids with over 90% probability (Fig. S1B). These PDOTS were assembled within one week and had a size of over 200 microns (Fig. 1C and D).

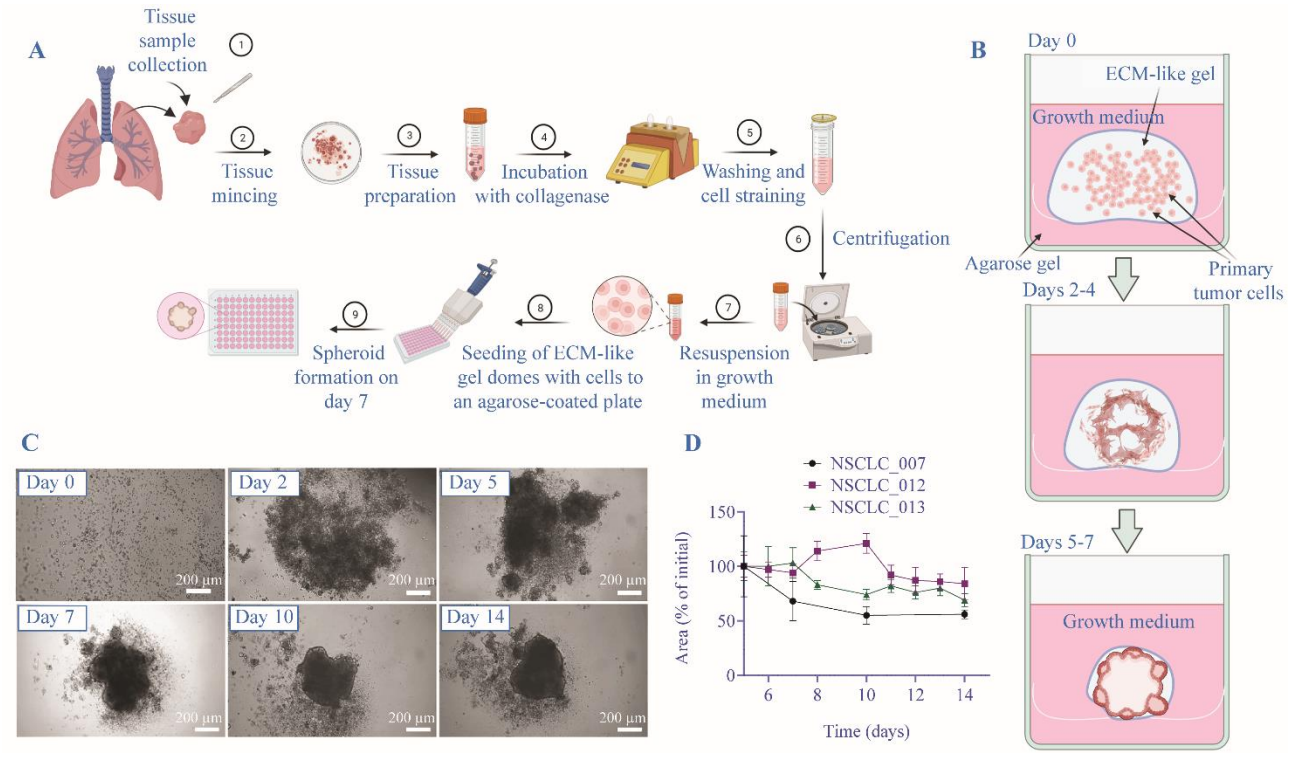

Fig. 1. Generation of free-floating NSCLC PDOTS. (A) Schematic representation of the free-floating PDOTS generation process. (B) Main stages of morphological changes during free-floating spheroid formation. Biorender software (https://biorender.com/) was used to create figures (A) and (B). (C) Time-lapse monitoring of spheroid morphological changes in transmitted light. (D) Kinetics of PDOTS area change over time for NSCLC_007, NSCLC_012, NSCLC_013, measured using brightfield images. The data are expressed as the mean ± SD. NSCLC, Non-small cell lung cancer; PDOTS, patient-derived organotypic tumor spheroid.

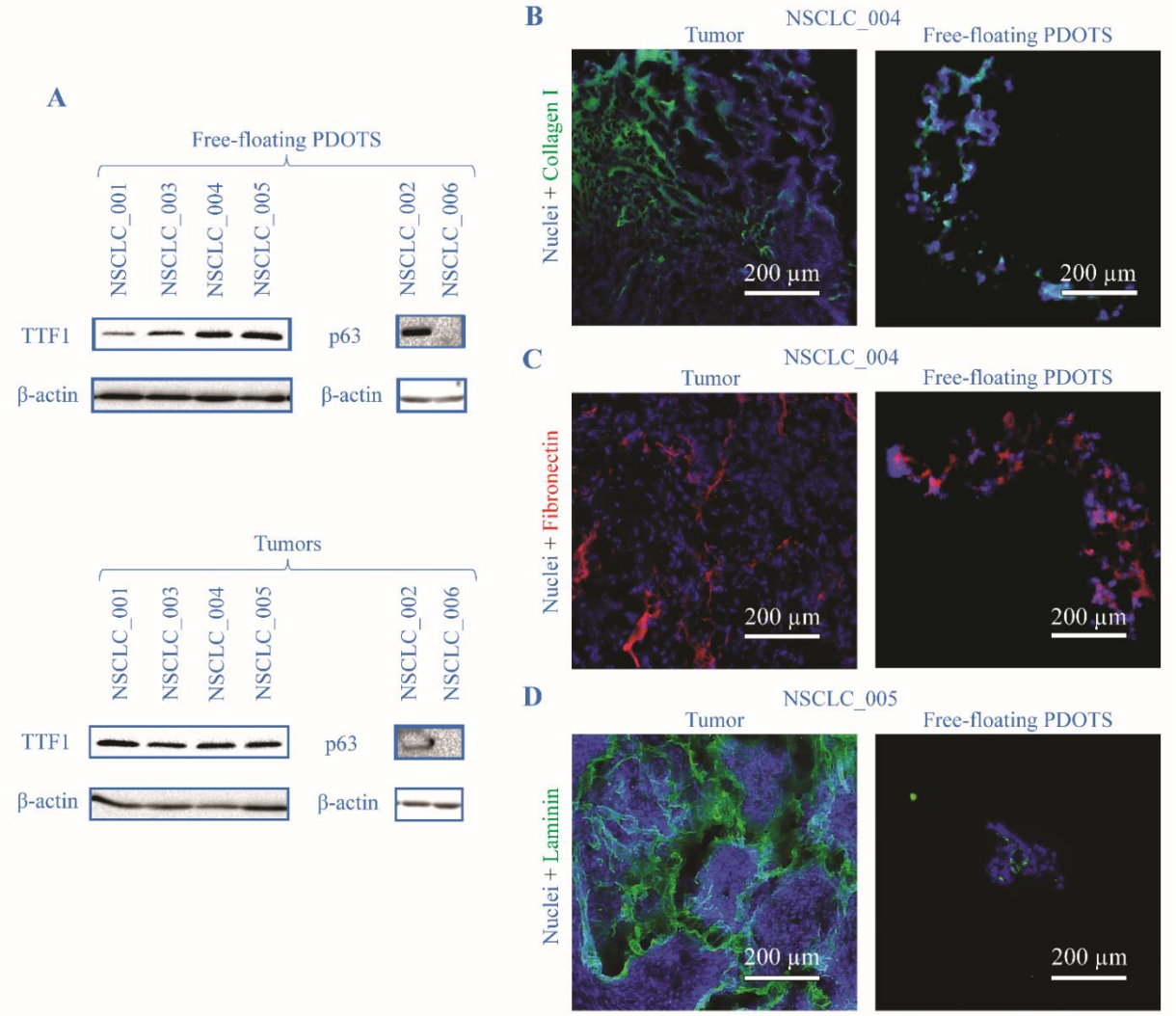

Fig. 2. Characterization of free-floating NSCLC PDOTS. (A) Immunoblotting analysis indicated the presence of lung adenocarcinoma-specific marker TTF1 and squamous-cell carcinoma-specific marker p63 (and its absence in large-cell carcinoma NSCLC_006) in the spheroids obtained from the corresponding NSCLC tumors. (B-D) IHC analysis of ECM distribution in NSCLC tumors and PDOTS. Collagen I (green) (B), fibronectin (red) (C), and laminin (green) (D) were detected in both tumors and free-floating PDOTS. DAPI staining indicates cell nuclei (blue). NSCLC, Non-small cell lung cancer; PDOTS, patient-derived organotypic tumor spheroid; TTF1, thyroid transcription factor 1; IHC, immunohistochemistry; ECM, extracellular matrix; DAPI, 4′,6-diamidino-2-phenylindole.

To confirm the preservation of tumor-specific, proliferative, and tissue integrity markers in PDOTS, we conducted immunoblotting analysis and immunohistochemistry (IHC) staining. Immunoblotting analysis of the obtained PDOTS indicated the retention of adenocarcinoma- or SCC-specific markers TTF1 and p63 (19), respectively (Fig. 2A). To further understand the integrity of free-floating spheroids, we examined the expression of ECM components and E-cadherin, an adhesion molecule primarily involved in the adhesion of epithelial cells to one another (20). IHC staining has shown that, similar to the parental tumors, free-floating PDOTS produce stromal ECM proteins such as collagen I, and basement membrane-specific proteins including fibronectin and laminin (Fig. 2B-D). As a part of the tumor microenvironment, ECM can significantly contribute to enhanced chemoresistance by acting as a steric barrier to the diffusion of therapeutic agents (21) and by promoting pro-survival signaling (6). All tested samples of free-floating PDOTS displayed the expression of E-cadherin that could mediate cellular contacts (Fig. S2), suggesting the retention of tissue integrity. In addition, the presence of Ki-67-positive staining in one-week-old PDOTS (Fig. S3) confirms ongoing proliferation, as Ki-67 is a well-established and widely accepted marker of cell proliferation.

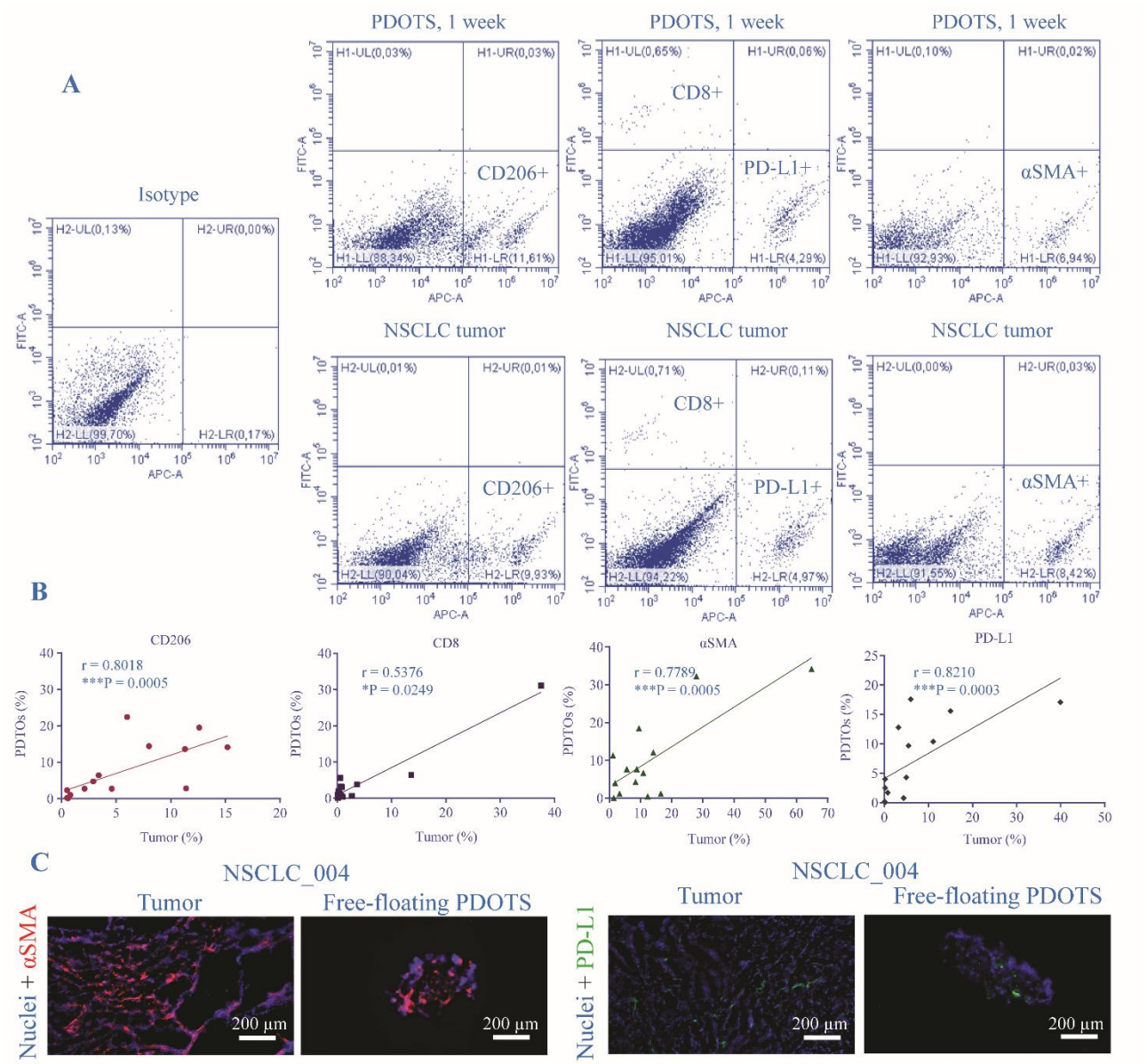

Fig. 3. Cell composition of free-floating NSCLC PDOTS. (A) Gating of CD206+, PD-L1+, αSMA+, and CD8+ cells, isolated from original tumors or PDOTS. (B) Pearson's correlations between cell compositions of PDOTS and parental tumors. Pearson's correlation coefficients and *P*-values were determined. (C) IHC images of αSMA+ (red) and PD-L1+ (green) cells in NSCLC tumors and free-floating spheroids. DAPI staining indicates cell nuclei (blue). NSCLC, Non-small cell lung cancer; PDOTS, patient-derived organotypic tumor spheroid; IHC, immunohistochemistry; CD206, cluster of differentiation 206, or mannose receptor; PD-L1, programmed death-ligand 1; α-SMA, α-smooth muscle actin; CD8, cluster of differentiation 8, a co-receptor for the T-cell receptor; DAPI, 4′,6-diamidino-2-phenylindole.

Cell composition of free-floating NSCLC PDOTS

To evaluate the expression of cell type-specific markers and compare the cellular composition of the PDOTS with the original tumors, we performed flow cytometry analysis. For cell phenotyping, four cell-specific markers were used (Fig. 3A). First, the percentage of cells expressing CD206, a marker of M2 tumor-associated macrophages, was determined. These cells are known to promote tumor growth, angiogenesis, and immunosuppression through the secretion of anti-inflammatory cytokines and remodeling of the tumor microenvironment (22). Next, the enrichment of the patient tumors and PDOTS with CD8+ T-cells and myofibroblasts expressing αSMA was defined. In NSCLC, CD8+ T-cells are key mediators of anti-tumor immunity, while myofibroblasts contribute to immunosuppression and tumor progression through extracellular matrix remodeling and cytokine secretion (23). Finally, the fraction of PD-L1-positive cells was evaluated. In the

tumor microenvironment, PD-L1 can be expressed by cancer cells and immune cells (24), and its expression level has been previously considered a prognostic marker in NSCLC (25). It was found that free-floating PDOTS retain immune and stromal cells. Moreover, percentages of CD8+, CD206+, PD-L1+, and αSMA+ cells correlated between spheroids and the original tumors (Fig. 3B). IHC staining of tumor and spheroid sections also confirmed the presence of αSMA+ and PD-L1+ in both specimens (Fig. 3C). Thus, the obtained results display the similarity of cell compositions between free-floating PDOTS and the parental tumors.

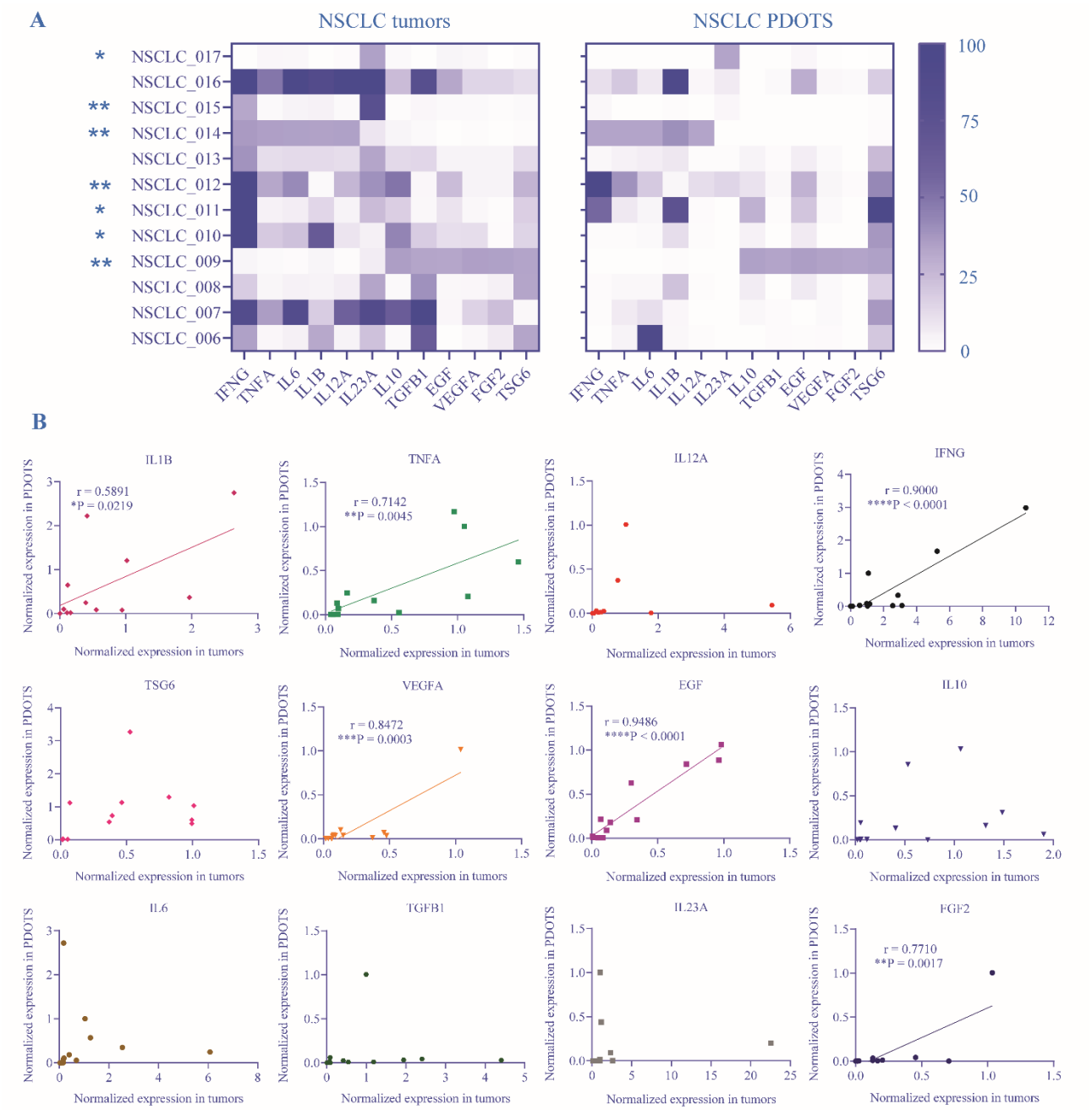

Fig. 4. Gene expression profiles of cytokines and growth factors in the free-floating NSCLC PDOTS and the parental tumors. (A) Heatmaps of normalized cytokine and growth factor gene expression profiles in NSCLC tumors and spheroids. indicates Pearson correlation analysis revealed statistically significant correlations between tumors and free-floating PDOTS in 7 out of 12 samples (*$P < 0.05$ and **$P < 0.01$) (see also Table S3). (B) Pearson correlations between cytokine/growth factor expression in PDOTS and the parental tumors. Pearson's correlation coefficients and P-values were determined for each gene (see also Table S4). NSCLC, Non-small cell lung cancer; PDOTS, patient-derived organotypic tumor spheroid.

Comparison of cytokine and growth factor expression profiles in PDOTS and parental tumors

To compare the expression of secretory biomarkers between PDOTS and the original tumors, we assessed the levels of 12 genes encoding cytokines and growth factors (interferon gamma (IFNG), tumor necrosis factor alpha (TNFA), interleukin (IL)6, IL1B, IL12A, IL23A, IL10, transforming growth factor-beta (TGFB), epidermal growth factor (EGF), vascular endothelial growth factor A (VEGFA), TNF-stimulated gene-6 protein (TSG6), and fibroblast growth factor 2 (FGF2)), all of which play important roles in the NSCLC tumor microenvironment. RT-PCR analysis revealed notable variations in the expression profiles of these cytokines and growth factors among NSCLC tumors and their corresponding free-floating spheroids (Fig. 4A). Considering separate samples, the expression profile correlated between free-floating PDOTS and the original tumors in 7 of 12 patients, indicating a high extent of immune microenvironment mimicking in 3D culture (Fig. 4A and Table S3).

Considering separate cytokines and growth factors, the correlations in gene expression between tumors and PDOTS were found for six specific genes, including EGF, VEGFA, IL1B, IFNG, TNFA, and FGF2 (Fig. 4B and Table S4). Thus, reproducing cytokine/growth factor expression profiles in free-floating spheroids might be important for their use in the tumor-immune cell crosstalk studies.

Anticancer drug response of free-floating NSCLC PDOTS

To demonstrate the feasibility of using free-floating NSCLC PDOTS for personalized drug sensitivity analysis, we evaluated their viability after exposure to five of the most commonly used chemotherapeutics, including cisplatin, etoposide, pemetrexed, paclitaxel, and gemcitabine. Notably, the process of spheroid generation and viability assay after drug exposure took ten days, which could be considered a clinically relevant term.

Analysis of drug sensitivity indicated a broad diversity in IC_{50} values for different drugs across free-floating PDOTS from ten patients (Fig. 5A and B). In some cases, IC_{50} values surpassed clinically relevant maximum concentrations (C_{max}) (26) for some drugs, indicating these spheroids to be resistant to certain drugs (Fig. S4). Interestingly, some free-floating spheroids, such as NSCLC_008, NSCLC_009, NSCLC_010, and NSCLC_011, displayed relatively high sensitivity to all tested drugs. However, in most cases, the spheroids exhibited resistance to at least one drug. Importantly, no cases of complete PDOTS drug resistance to all drugs were observed among the PDOTS.

In this regard, *in vitro* patient-derived tumor models can be a valuable tool for personalized assessment of chemotherapeutic efficacy.

Analysis of PDOTS drug resistance

To understand the possible cause of drug response variation, the mRNA expression levels of cytochrome P450 (CYP) and ATP-binding cassette (ABC) transporters were measured, which can mediate drug resistance. Some CYPs make anticancer drugs more soluble and less toxic by oxidizing them (27), while transporters actively pump chemotherapy drugs out of cancer cells, thereby reducing their efficacy (28).

Although PCR analysis demonstrated a similarity in CYP expression levels between PDOTS and the original tumors (Fig. 6A), we did not find any trends in the expression of different CYPs and resistance to certain drugs (Fig. 6B and C). As for ABC transporter expression, we identified several interesting findings (Fig. 6D and D). For instance, NSCLC_012 spheroids with the highest ABCC5 expression are resistant to pemetrexed. Indeed, ABCC5 was shown to mediate the inherited resistance to pemetrexed in several cancers (29). According to our data, NSCLC_003 spheroids with the highest ABCG2 expression are more resistant to cisplatin. These data are consistent with the results of previous studies demonstrating that different ABCG2-overexpressing tumors, including NSCLC, are resistant to this drug (30). Interestingly, we observed substantial variation in CYP and ABC expression across NSCLC PDOTS from different patients (Fig. 6B-E), which likely contributes to individual differences in resistance to chemotherapeutics.

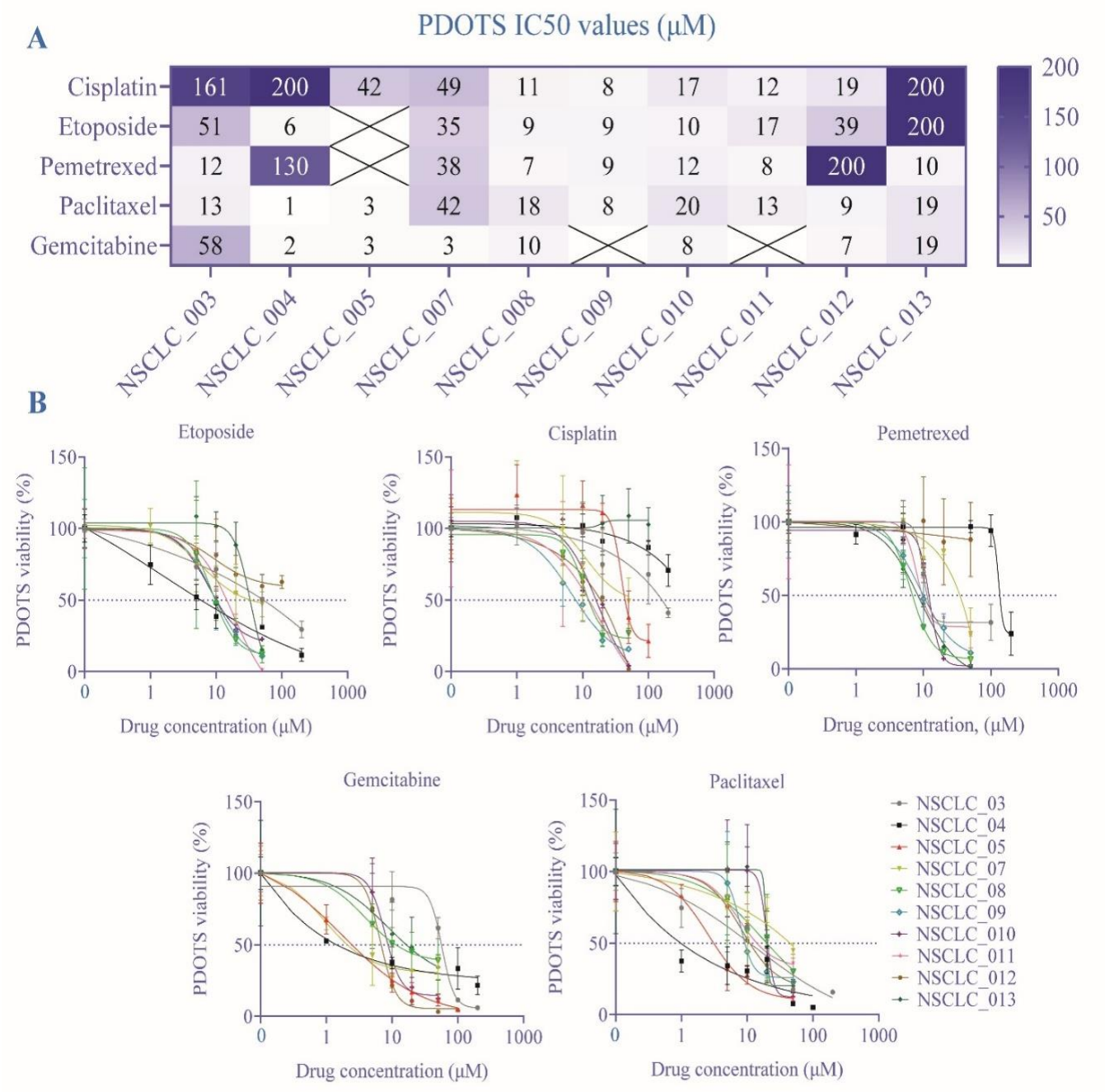

Fig. 5. Drug sensitivity profiling of free-floating NSCLC PDOTS. (A) A heatmap of cisplatin, paclitaxel, gemcitabine, etoposide, and pemetrexed IC_{50}s, determined for free-floating PDOTS from ten NSCLC patients. (B) Drug dose-dependent survival curves for free-floating PDOTS from ten NSCLC patients (see also Fig. S2). Data are presented as mean ± SD, n = 3. NSCLC, Non-small cell lung cancer; PDOTS, patient-derived organotypic tumor spheroid.

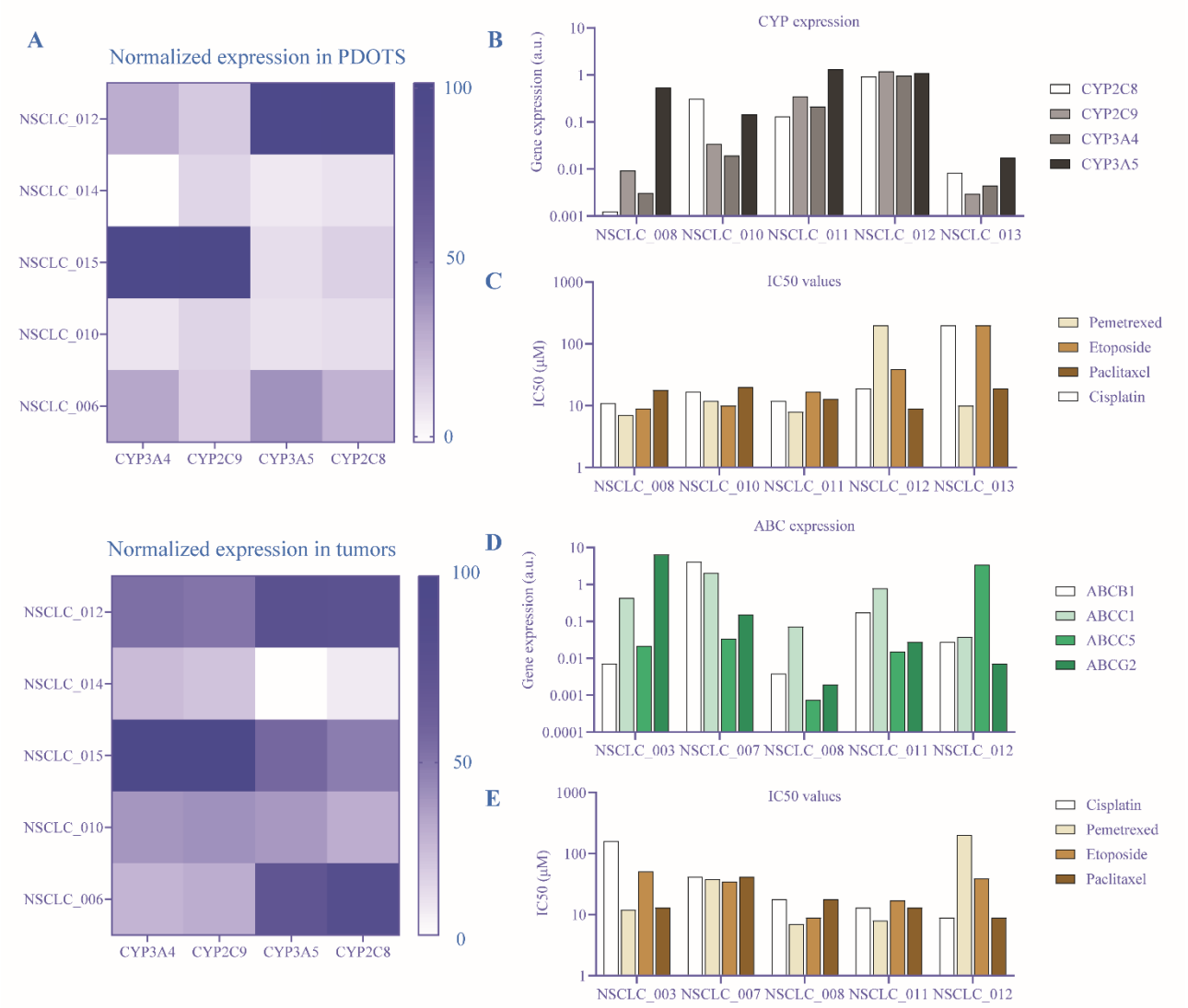

Fig. 6. Analysis of drug resistance gene expression in free-floating NSCLC PDOTS. (A) Heatmaps of CYP gene expression profiles in the NSCLC tumors and spheroids. (B) CYP gene expression levels in free-floating PDOTS versus (C) IC_{50} values of chemotherapeutics in them. (D) ABC gene expression levels in free-floating PDOTS versus (E) IC_{50} values of chemotherapeutics in them. Data are expressed as means, n = 3. NSCLC, Non-small cell lung cancer; PDOTS, patient-derived organotypic tumor spheroid; CYP, cytochrome P450; ABC, ATP-binding cassette transporters.

DISCUSSION

PDTOs/PDOTS have emerged as a promising tool in personalized medicine for drug screening purposes. Several studies have demonstrated the retention of the histological and genetic characteristics of primary tumors (31) and the high prognostic value of NSCLC PDTO/PDOTS models (32-35). At the same time, earlier reports have noted certain issues related to the production of lung cancer 3D multicellular models and their properties, such as low generation success rate (32,36,37), fibroblast and normal epithelium overgrowth (38), loss of immune components over time (12), and the need for long-term cultivation before drug testing (32). The primary goal of this study was to generate and characterize free-floating PDOTS, obtained using a new technique (Fig. 1A and B), in light of these reported issues.

The use of stimuli-responsive ECM-mimicking gels and non-adhesive coatings allows for the generation of free-floating PDOTS within one week (Fig. 1C and D), whereas the traditional method of culturing in MatrigelTM or similar ECM-like gel typically requires a longer time for PDTO/PDOTS formation (10). The speed of intercellular contact formation during organoid or spheroid assembly likely plays a critical role in their successful establishment. It has been shown

that cell aggregation in tumor spheroids is mediated by E- and N-cadherins, which are key contributors to pro-survival signaling and drug resistance (39). Rapid reformation of functional E-cadherin junctions is essential for the survival of both normal epithelial and cancer cells derived from highly differentiated carcinomas (40,41). While E-cadherin expression was confirmed at the protein level in all tested samples of free-floating spheroids (Fig. S2), the accelerated restoration of cell-cell interactions during spheroid formation may explain the significantly higher establishment success rate of over 90% (Fig. S1B) compared to the 40-70% success rates typically reported for conventional NSCLC organoids (32,33,35-37).

Fast assembly of free-floating spheroids appears to be important not only for their survival but also for better mimicking the tumor microenvironment. In PDTO models, it has been shown that long-term organoid cultivation often results in the overgrowth of stromal cells, such as cancer-associated fibroblasts (42), or the loss of immune cells due to their limited expansion capacity (16). While the deficiency of immune cells can be addressed by adding them to the tumor organoid culture (43), overcoming contamination with fibroblasts remains more challenging (37). This problem can be partly solved by filtering out large stromal cell clusters before starting the organoid culture and by adjusting the growth medium to slow down the growth of normal lung organoids (32). The free-floating PDOTS showed expression of cancer cell-specific NSCLC markers (Fig. 2B) as well as ECM components of connective tissue (collagen I) and basement membrane (laminin and fibronectin) (Fig. 2C-E). Flow cytometry analysis demonstrated a strong correlation in the proportion of αSMA-positive fibroblasts between the original tumors and PDOTS without evidence of fibroblast overgrowth (Fig. 3B and C). Additionally, PD-L1+ cells, CD8+ T-cells, and CD206+ macrophages were retained in the free-floating PDOTS at levels similar to those observed in the parental tumors (Fig. 3B and C).

A unique pattern of cytokine and growth factor expression profile in a tumor strongly affects tumor growth and the development of immune tolerance. Multiple growth factors, cytokines, and their receptors are considered significant prognostic NSCLC biomarkers (44). We first evaluated whether PDOTS reproduce growth factor/cytokine expression in the parental NSCLC tumors. It turned out that the expression profile in free-floating PDOTS correlated with the parental tumors in 58% of samples (7 of 12; Fig. 4A). Significant correlations were found for six growth factor and cytokine genes, including IL1B, IFNG, EGF, VEGFA, FGF2, and TNFA (Fig. 4B). These cytokines and growth factors significantly contribute to NSCLC progression and can be produced by various cell types in the tumor microenvironment, including cancer cells, fibroblasts, and immune cells (45). For instance, EGF binds to and activates the EGFR receptor, which is associated with NSCLC tumor growth and increased survival rate (46). FGF2 and VEGFA are both growth factors that contribute to tumor angiogenesis (44). TNFα and its receptor are prognostic biomarkers for NSCLC, which is associated with increased drug resistance and poor outcome (47). IL-1β, a proinflammatory cytokine from the IL-1 family, contributes to tumor cell proliferation, pro-survival signaling, migration, and chemoresistance in NSCLC (48). Finally, the proinflammatory cytokine IFNγ activates the STAT1 transcription factor in lung adenocarcinoma cells, leading to PD-L1 upregulation and the acquisition of immune tolerance (49).

Thus, free-floating spheroids exhibited a relatively high similarity to the parental tumors in terms of morphology, cell composition, and growth factor/cytokine expression profile. Therefore, the developed spheroid tumor model could be a valuable tool for personalized analysis of drug sensitivity.

Despite significant advances in targeted therapies and immunotherapeutic strategies, chemotherapy remains the primary first-line treatment option for advanced NSCLC in European countries (5). The gold standard for NSCLC chemotherapy involves a platinum-based doublet, combining cisplatin (or carboplatin) with another cytostatic drug such as pemetrexed, gemcitabine, etoposide, or paclitaxel. Although tumor responsiveness to

chemotherapy is highly variable and treatment often carries a high risk of adverse effects, no reliable genetic biomarkers are currently available to predict its efficacy (50). In this context, the use of PDTOs/PDOTS to personalize chemotherapy represents a promising approach.

Our data confirm a broad variation in drug sensitivity across free-floating PDOTS from different patients, reaching up to two orders of magnitude in IC_{50} value (Fig. 5). Some PDOTS exhibited very high IC_{50} values for certain drugs, suggesting resistance to those treatments (Fig. S4). Several factors may contribute to the observed variation in drug response. One important factor is the difference in the expression of genes involved in drug resistance, including CYP enzymes and ABC transporters (27,28). According to our data, free-floating PDOTS exhibited a high degree of similarity in CYP expression compared to the original tumors (Fig. 6A). However, significant variation in CYP and ABC expression across PDOTS from different NSCLC patients was observed (Fig. 6B-E), highlighting the importance of evaluating individual drug resistance to optimize therapeutic outcomes. In this context, the use of PDOTS appears highly promising for the personalized selection of chemotherapeutic agents. At least, it could assist in choosing the second drug to pair with cisplatin or carboplatin in a platinum-based doublet regimen. Moreover, PDOTS could serve as a useful platform for testing ABC (51) and CYP (52) inhibitors developed to overcome resistance to multiple cytostatic drugs.

It should be noted that in this study, we generated free-floating spheroids from surgically resected tumor tissue and maintained them under short-term culture conditions. Consequently, the assessment of PDOTS drug sensitivity in this context is primarily applicable to guiding adjuvant therapy decisions. In contrast, PDTOs enable the generation of 3D cultures from limited tissue obtained through minimally invasive biopsies. These cultures support long-term expansion, serial passaging, and cryopreservation, enabling their use in neoadjuvant therapy selection and biobanking (7). Therefore, further optimization is needed to adapt free-floating PDOTS protocols for use with biopsy-derived material, facilitating their potential role in preoperative treatment planning. Another limitation of PDOTS is their rapid evolution following establishment. Cultivation conditions can markedly influence the viability and proliferation rates of various cell types and cancer cell clones, leading to significant shifts in cell composition and clonality over time. While this approach enables rapid processing and analysis, it may present limitations in terms of long-term usability and scalability.

CONCLUSION

This study aimed to investigate the properties of NSCLC PDOTS generated using a free-floating method. This technique offers a high success rate in establishing spheroids and accelerating assembly, allowing the time between tumor tissue acquisition and drug testing to be reduced to as short as ten days. The free-floating spheroids preserved key similarities to the parental tumors, including morphology, ECM, and cell composition, and cytokine/growth factor expression profiles. These characteristics make the obtained PDOTS a valuable tool for various applications, including cancer research and personalized drug testing, which can be exploited for the management of adjuvant chemotherapy, as discussed in this study. Future directions may include optimizing PDOTS protocols for use with biopsy-derived material to support preoperative treatment planning, as well as adapting them for longer cultivation to allow immunotherapeutic testing. We believe that the growing evidence supporting the benefits of PDOTS/PDTOs for personalized treatment, coupled with ongoing advancements in production techniques, will facilitate the clinical translation of this promising technology.

Acknowledgements

This work was supported by the Ministry of Science and Higher Education of the Russian Federation within the framework of state support for the creation and development of a World-Class Research Center “Digital Biodesign and Personalized Healthcare”, project No. 075-15-2022-306.

Conflict of interest statement

The authors declared no conflict of interest in this study.

Authors' contributions

The work reported in the paper has been performed by the authors, unless specified in the text. L. Ismail contributed to investigation, data curation, formal analysis, methodology, validation, visualization, and writing of the original draft and its review and editing; K. Zahid was involved in investigation, data curation, formal analysis, methodology, and contributed to writing the original draft and its review and editing; A. Polyanskaya, A. Al Othman, N. Shen, X. Qi participated in writing the original draft and in reviewing and editing the manuscript; R. Sulimanov, Y. Esakov contributed to writing the original draft, reviewing and editing the manuscript, and provided resources; V. Makarov contributed to writing the original draft, manuscript review and editing, resource provision, and funding acquisition; G. Filkov and A. Trofimenko participated in reviewing and editing the manuscript, provided resources, and was involved in project administration; A. Mezentsev contributed to conceptualization, data curation, formal analysis, methodology, investigation, validation, visualization, and writing the original draft and its review and editing; M. Durymanov was responsible for conceptualization, supervision, investigation, methodology, visualization, project administration, and writing the original draft and its review and editing. All authors read and approved the finalized article.

Ethics approval and consent to participate

All procedures were performed in line with the ethical standards of the institutional research committee and conform to the 1964 Helsinki Declaration and its later amendments or comparable ethical standards. Informed consent was obtained from all patients before tissue acquisition, and they were informed of the potential risks and benefits of participating in the study. The research plan received approval from the Ethics Committee of the City Clinical Oncological Hospital No. 1 (Moscow, Russia) on 09/02/2024 (approval reference No. 2).

REFERENCES

1. Garinet S, Wang P, Mansuet-Lupo A, Fournel L, Wislez M, Blons H. Updated prognostic factors in localized NSCLC. Cancers (Basel). 2022;14(6):1400,1-20. DOI: 10.3390/cancers14061400.
2. Mezentsev A, Durymanov M, Makarov VA. A Comprehensive review of protein biomarkers for invasive lung cancer. Curr Oncol. 2024;31(9):4818-4854. DOI: 10.3390/curroncol31090360.
3. Poddubskaya E, Bondarenko A, Boroda A, Zotova E, Glusker A, Sletina S, *et al*. Transcriptomics-guided personalized prescription of targeted therapeutics for metastatic ALK-positive lung cancer case following recurrence on ALK inhibitors. Front Oncol. 2019;9:1026,1-8. DOI: 10.3389/fonc.2019.01026.
4. Bepler G, Williams C, Schell MJ, Chen W, Zheng Z, Simon G, *et al*. Randomized international phase III trial of ERCC1 and RRM1 expression–based chemotherapy versus gemcitabine/carboplatin in advanced non–small-cell lung cancer. J Clin Oncol. 2013;31(19):2404-2412. DOI: 10.1200/JCO.2012.46.9783.
5. Bailey H, Lee A, Eccles L, Yuan Y, Burlison H, Forshaw C, *et al*. Treatment patterns and outcomes of patients with metastatic non-small cell lung cancer in five european countries:a real-world evidence survey. BMC Cancer. 2023;23(1):603,1-20. DOI: 10.1186/s12885-023-11074-z.
6. Rozenberg JM, Filkov GI, Trofimenko AV, Karpulevich EA, Parshin VD, Royuk VV, *et al*. Biomedical applications of non-small cell lung cancer spheroids. Front Oncol. 2021;11:791069,1-13. DOI: 10.3389/fonc.2021.791069.
7. Durymanov M. Tumor spheroids, tumor organoids, tumor explants, and tumoroids: what are the differences between them? Biochemistry (Mosc.). 2025;9(2):200-213. DOI: 10.1134/S0006297924604234.
8. Surina, Tanggis, Suzuki T, Hisata S, Fujita K, Fujiwara S, *et al*. Patient-derived spheroids and patient-derived organoids simulate evolutions of lung cancer. Heliyon. 2023;9(3):e13829,1-14. DOI: 10.1016/j.heliyon.2023.e13829.
9. Lee SH, Hu W, Matulay JT, Silva MV, Owczarek TB, Kim K, *et al*. Tumor evolution and drug response in patient-derived organoid models of bladder cancer. Cell. 2018;173(2):515-528. DOI: 10.1016/j.cell.2018.03.017.
10. Sachs N, Papaspyropoulos A, Zomer-van Ommen DD, Heo I, Böttinger L, Klay D, *et al*. Long-term expanding human airway organoids for disease modeling. EMBO J. 2019;38(4):e100300,1-20. DOI: 10.15252/embj.2018100300.
11. Di Liello R, Ciaramella V, Barra G, Venditti M, Della Corte CM, Papaccio F, *et al*. *Ex vivo* lung cancer spheroids resemble treatment response of a patient with NSCLC to chemotherapy and

immunotherapy:case report and translational study. ESMO Open. 2019;4(4):e000536,1-6. DOI: 10.1136/esmoopen-2019-000536.
12. Neal JT, Li X, Zhu J, Giangarra V, Grzeskowiak CL, Ju J, *et al*. Organoid modeling of the tumor immune microenvironment. Cell. 2018;175(7):1972-1988. DOI: 10.1016/j.cell.2018.11.021.
13. Gunti S, Hoke ATK, Vu KP, London NR. Organoid and spheroid tumor models: techniques and applications. Cancers (Basel). 2021;13:874,1-17. DOI: 10.3390/cancers13040874.
14. Ivanova E, Kuraguchi M, Xu M, Portell AJ, Taus L, Diala I, *et al*. Use of *ex vivo* patient-derived tumor organotypic spheroids to identify combination therapies for Her2 mutant non–small cell lung cancer. Clin Cancer Res. 2020;26(10):2393-2403. DOI: 10.1158/1078-0432.CCR-19-1844.
15. Zhang Z, Wang H, Ding Q, Xing Y, Xu Z, Lu C, *et al*. Establishment of patient-derived tumor spheroids for non-small cell lung cancer. PLoS One. 2018;13(3):e0194016,1-8. DOI: 10.1371/journal.pone.0194016.
16. Verduin M, Hoeben A, De Ruysscher D, Vooijs M. Patient-derived cancer organoids as predictors of treatment response. Front Oncol. 2021;11:641980,1-16. DOI: 10.3389/fonc.2021.641980.
17. Qi X, Prokhorova AV, Mezentsev AV, Shen N, Trofimenko AV, Filkov GI, *et al*. Comparison of EMT-related and multi-drug resistant gene expression, extracellular matrix production, and drug sensitivity in NSCLC spheroids generated by scaffold-free and scaffold-based methods. Int J Mol Sci. 2022;23(21):13306,1-12. DOI: 10.3390/ijms232113306.
18. Sulimanov R, Koshelev K, Makarov V, Mezentsev A, Durymanov M, Ismail L, *et al*. Mathematical modeling of non-small-cell lung cancer biology through the experimental data on cell composition and growth of patient-derived organoids. Life (Basel). 2023;13(11):2228,1-10. DOI: 10.3390/life13112228.
19. Travis WD, Brambilla E, Nicholson AG, Yatabe Y, Austin JH, Beasley MB, *et al*. The 2015 world health organization classification of lung tumors:impact of genetic, clinical and radiologic advances since the 2004 classification. J Thorac Oncol. 2015;10(9):1243-1260. DOI: 10.1097/JTO.0000000000000630.
20. Takeichi M. Cadherin cell adhesion receptors as a morphogenetic regulator. Science. 1991;251(5000): 1451-1455. DOI: 10.1126/science.2006419.
21. Durymanov MO, Rosenkranz AA, Sobolev AS. Current approaches for improving intratumoral accumulation and distribution of nanomedicines. Theranostics. 2015;5(9):1007-1020. DOI: 10.7150/thno.11742.
22. Dong P, Ma L, Liu L, Zhao G, Zhang S, Dong L, *et al*. CD86+/CD206+, diametrically polarized tumor-associated macrophages, predict hepatocellular carcinoma patient prognosis. Int J Mol Sci. 2016;17(3):320,1-12. DOI: 10.3390/ijms17030320.
23. Kalluri R. The biology and function of fibroblasts in cancer. Nat Rev Cancer. 2016;16(9):582-598. DOI: 10.1038/nrc.2016.73.
24. Cha JH, Chan LC, Li CW, Hsu JL, Hung MC. Mechanisms controlling PD-L1 expression in cancer. Mol Cell. 2019;76(3):359-370. DOI: 10.1016/j.molcel.2019.09.030.
25. Li H, Xu Y, Wan B, Song Y, Zhan P, Hu Y, *et al*. The clinicopathological and prognostic significance of PD-L1 expression assessed by immunohistochemistry in lung cancer: a meta-analysis of 50 studies with 11,383 patients. Transl Lung Cancer Res. 2019;8(4):429-449. DOI: 10.21037/tlcr.2019.08.04.
26. Liston DR, Davis M. Clinically relevant concentrations of anticancer drugs: a guide for nonclinical studies. Clin Cancer Res. 2017;23(14):3489-3498. DOI: 10.1158/1078-0432.CCR-16-3083.
27. Kaur G, Gupta SK, Singh P, Ali V, Kumar V, Verma M. Drug-metabolizing enzymes: role in drug resistance in cancer. Clin Transl Oncol. 2020;22(10):1667-1680. DOI: 10.1007/s12094-020-02325-7.
28. Robey RW, Pluchino KM, Hall MD, Fojo AT, Bates SE, Gottesman MM. Revisiting the role of ABC transporters in multidrug-resistant cancer. Nat Rev Cancer. 2018;18(7):452-464. DOI: 10.1038/s41568-018-0005-8.
29. Sun JM, Oh DY, Lee SH, Kim DW, Im SA, Kim TY, *et al*. The relationship between response to previous systemic treatment and the efficacy of subsequent pemetrexed therapy in advanced non-small cell lung cancer. Lung Cancer. 2010;68(3):427-32. DOI: 10.1016/j.lungcan.2009.07.013.
30. Niu Q, Wang W, Li Y, Ruden DM, Wang F, Li Y, *et al*. Low molecular weight heparin ablates lung cancer cisplatin-resistance by inducing proteasome-mediated ABCG2 protein degradation. PLoS One. 2012;7(7):e41035,1-9. DOI: 10.1371/journal.pone.0041035.
31. Chen JH, Chu XP, Zhang JT, Nie Q, Tang WF, Su J, *et al*. Genomic characteristics and drug screening among organoids derived from non-small cell lung cancer patients. Thorac Cancer. 2020;11(8): 2279-2290. DOI: 10.1111/1759-7714.13542.
32. Hu Y, Sui X, Song F, Li Y, Li K, Chen Z, *et la*. Lung cancer organoids analyzed on microwell arrays predict drug responses of patients within a week. Nat Commun. 2021;12(1):2581,1-14. DOI: 10.1038/s41467-021-22676-1.
33. Koga T, Soh J, Hamada A, Miyano Y, Fujino T, Obata K, *et al*. Clinical relevance of patient-derived organoid of surgically resected lung cancer as an *in vitro* model for biomarker and drug testing. JTO Clin Res Rep. 2023;4(9):100554,1-11. DOI: 10.1016/j.jtocrr.2023.100554.
34. Kim SY, Kim SM, Lim S, Lee JY, Choi SJ, Yang SD, *et al*. Modeling clinical responses to targeted therapies by patient-derived organoids of

advanced lung adenocarcinoma. Clin Cancer Res. 2021;27(15):4397-4409.
DOI: 10.1158/1078-0432.CCR-20-5026.
35. Wang HM, Zhang CY, Peng KC, Chen ZX, Su JW, Li YF, *et al*. Using patient-derived organoids to predict locally advanced or metastatic lung cancer tumor response:a real-world study. Cell Rep Med. 2023;4(2):100911,1-22.
DOI: 10.1016/j.xcrm.2022.100911.
36. Della Corte CM, Barra G, Ciaramella V, Di Liello R, Vicidomini G, Zappavigna S, *et al*. Antitumor activity of dual blockade of PD-L1 and MEK in NSCLC patients derived three-dimensional spheroid cultures. J Exp Clin Cancer Res. 2019;38(1):253,1-12.
DOI: 10.1186/s13046-019-1257-1.
37. Dijkstra KK, Monkhorst K, Schipper LJ, Hartemink KJ, Smit EF, Kaing S, *et al*. Challenges in establishing pure lung cancer organoids limit their utility for personalized medicine. Cell Rep. 2020;31(5):107588,1-13.
DOI: 10.1016/j.celrep.2020.107588.
38. Si LL, Lv L, Zhou WH, Hu WD. Establishment and identification of human primary lung cancer cell culture *in vitro*. Int J Clin Exp Pathol. 2015;8(6):6540-6546.
PMID: 26261533.
39. Lin RZ, Chou LF, Chien CCM, Chang HY. Dynamic analysis of hepatoma spheroid formation: roles of E-cadherin and beta1-integrin. Cell Tissue Res. 2006;324(3):411-422.
DOI: 10.1007/s00441-005-0148-2.
40. Goncharova EA, Goncharov DA, James ML, Atochina-Vasserman EN, Stepanova V, Hong SB, *et al*. Folliculin controls lung alveolar enlargement and epithelial cell survival through E-cadherin, LKB1, and AMPK. Cell Rep. 2014;7(2):412-423.
DOI: 10.1016/j.celrep.2014.03.025.
41. Manuel Iglesias J, Beloqui I, Garcia-Garcia F, Leis O, Vazquez-Martin A, Eguiara A, *et al*. Mammosphere formation in breast carcinoma cell lines depends upon expression of E-cadherin. PLoS One. 2013;8(10):e77281,1-12.
DOI: 10.1371/journal.pone.0077281.
42. Ko YR, Kim JM, Kang Y, Kim M, Jang SJ. A method for culturing patient-derived lung cancer organoids from surgically resected tissues and biopsy samples. Organoid. 2022 2:e19,1-9.
DOI: 10.51335/organoid.2022.2.e19.
43. Dijkstra KK, Cattaneo CM, Weeber F, Chalabi M, van de Haar J, Fanchi LF, *et al*. Generation of tumor-reactive t cells by co-culture of peripheral blood lymphocytes and tumor organoids. Cell. 2018;174(6):1586-1598.
DOI: 10.1016/j.cell.2018.07.009.
44. Donnem T, Andersen S, Al-Saad S, Al-Shibli K, Busund LT, Bremnes RM. Prognostic impact of angiogenic markers in non–small-cell lung cancer is related to tumor size. Clin Lung Cancer. 2011;12(2):106-115.
DOI: 10.1016/j.cllc.2011.03.005.
45. Ramachandran S, Verma AK, Dev K, Goyal Y, Bhatt D, Alsahli MA, *et al*. Role of cytokines and chemokines in NSCLC immune navigation and proliferation. Oxid Med Cell Longev. 2021;2021:e5563746,1-20.
DOI: 10.1155/2021/5563746.
46. Bethune G, Bethune D, Ridgway N, Xu Z. Epidermal growth factor receptor (EGFR) in lung cancer:an overview and update. J Thorac Dis. 2010;2(1): 48-51.
PMID: 22263017.
47. Gong k, Gao G, Beckley N, Zhang Y, Yang X, Sharma M, *et al*. Tumor necrosis factor in lung cancer:complex roles in biology and resistance to treatment. Neoplasia. 2021;23(2):189-196.
DOI: 10.1016/j.neo.2020.12.006.
48. Garon EB, Chih-Hsin Yang J, Dubinett SM. The Role of interleukin 1β in the pathogenesis of lung cancer. JTO Clin Res Rep. 2020;1:100001,1-11.
DOI: 10.1016/j.jtocrr.2020.100001.
49. Stutvoet TS, Kol A, de Vries EG, de Bruyn M, Fehrmann RS, Terwisscha van Scheltinga AG, *et al*. MAPK pathway activity plays a key role in PD-L1 expression of lung adenocarcinoma cells. J Pathol. 2019;249(1):52-64.
DOI: 10.1002/path.5280.50. Szejniuk WM, Robles AI, McCulloch T, Falkmer UGI, Røe OD. Epigenetic predictive biomarkers for response or outcome to platinum-based chemotherapy in non-small cell lung cancer, current state-of-art. Pharmacogenomics J. 2019;19(1):5-14.
DOI: 10.1038/s41397-018-0029-1.
51. Budagaga Y, Sabet Z, Zhang Y, Novotná E, Hanke I, Rozkoš T, *et al*. Tazemetostat synergistically combats multidrug resistance by the unique triple inhibition of ABCB1, ABCC1, and ABCG2 efflux transporters *in vitro* and *ex vivo*. Biochem Pharmacol. 2023;216:115769.
DOI: 10.1016/j.bcp.2023.115769.
52. Zhou L, Chen W, Cao C, Shi Y, Ye W, Hu J, *et al*. Design and synthesis of α-naphthoflavone chimera derivatives able to eliminate cytochrome P450 (CYP)1B1-mediated drug resistance via targeted CYP1B1 degradation. Eur J Med Chem. 2020;189:112028,1-11.
DOI: 10.1016/j.ejmech.2019.112028.